

## **Electronic Supplementary Information (ESI).**

### **Zeolites catalyze the halogen exchange reaction of alkyl halides**

Paloma Mínguez-Verdejo,<sup>a</sup> Juan Carlos Hernández-Garrido,<sup>b</sup> Alejandro Vidal-Moya,<sup>a</sup>  
Judith Oliver-Meseguer<sup>\*a</sup> and Antonio Leyva-Pérez.<sup>\*a</sup>

<sup>a</sup> Instituto de Tecnología Química. Universitat Politècnica de València-Consejo Superior de Investigaciones Científicas. Avda. de los Naranjos s/n, 46022, València, Spain.

<sup>b</sup> Departamento de Ciencia de los Materiales e Ingeniería Metalúrgica y Química Inorgánica, Facultad de Ciencias, Universidad de Cádiz, Campus Universitario Puerto Real, 11510 Puerto Real, Cádiz, Spain.

Corresponding authors: joliverm@itq.upv.es, anleyva@itq.upv.es

#### **Table of Contents**

Experimental Section.....	ESI2
General.....	ESI2
Physicochemical techniques.....	ESI2
Solid state magic angle spinning nuclear magnetic resonance.....	ESI3
Electron microscopy.....	ESI3
Catalyst preparation.....	ESI4
General preparation of basic zeolites.....	ESI4
General preparation of acid zeolites.....	ESI4
General procedure ion-exchanged beta zeolites.....	ESI4
Typical reaction procedure in batch.....	ESI5
Calculation of the space-time yield (STY) .....	ESI5
Tables S1-S3.....	ESI6
Figures S1-S16.....	ESI8
References.....	ESI26
Characterization of compounds.....	ESI27

## Experimental Section.

**General.** Glassware was dried in an oven at 175 °C before use. Reactions were performed in 6-7 ml vials equipped with a magnetic stirrer and closed with a steel cap having a rubber septum part to sample out. Reagents and solvents were obtained from commercial sources and were used without further purification otherwise indicated.

### Physicochemical techniques.

- **Inductively coupled plasma-atomic emission spectroscopy (ICP-AES):** The metal content of the zeolites was determined after disaggregating the solids in aqueous HF and dilution before analysis.

- **Elemental analysis (EA):** The carbon, hydrogen, nitrogen and sulfur content of the samples was quantified with a Fisons EA 1108CHN-S analyzer.

- **Thermogravimetric analysis (TG):** Samples were subjected to a temperature ramp in the presence of a gas flow in a NETZSCH STA 449F3 STA449F3A-1625-M instrument.

- **Fourier Transformed Infrared (FT-IR) Spectroscopy:** Spectra were recorded on attenuated total reflection infrared spectroscopy, from 400 to 4000  $\text{cm}^{-1}$ , by dropping a small sample on the ATR crystal.

- **X-ray photoelectron spectroscopy (XPS):** Measurements were performed on a SPECS spectrometer equipped with a Phoibos 150 MCD-9 analyser using a non-monochromatic Mg KR (1,253.6 eV) X-ray source working at 50 W. The C1s peak has been set at 284.5 eV as the internal reference for the peak positions in the XPS spectra.

- **X-ray diffraction (XRD):** Spectra were recorded in a CubiX PRO (PAN Analytical) spectrometer, with a Cu K( $\alpha$ ) radiation source, 1.5406 Å wavelength.

- **Gas chromatography-mass spectrometry (GC-MS):** Gas chromatographic analyses were performed in an instrument equipped with a 25 cm capillary column of 5% phenylmethylsilicone. *N*-dodecane was used as an external standard. GC-MS analyses were performed on a spectrometer equipped with the same column as the GC and operated under the same conditions.

- **Liquid nuclear magnetic resonance (NMR):**  $^1\text{H}$ ,  $^{13}\text{C}$  and DEPT NMR spectra were recorded at room temperature on a 300.1 MHz spectrometer.

Products were characterised by GC-MS and NMR, and compared with the given literature.

**Solid state magic angle spinning nuclear magnetic resonance (SS-MAS NMR).**

Spectra were recorded at room temperature with a Bruker AVIII HD 400 WB spectrometer. The  $^{23}\text{Na}$  spectra were recorded with  $\pi/12$  pulse length of 1  $\mu\text{s}$ , and a recycle delay of 3s, pinning the samples at 20 kHz. The  $^1\text{H}/^{13}\text{C}$  cross polarization (CP) MAS spectra were recorded with a  $^1\text{H}$   $90^\circ$  pulse of 4.5 ms, a contact time of 3 ms and a recycle delay of 3 s, using a spin rate of 5 kHz.

**Electron microscopy.** Samples for electron microscopy studies were prepared by dropping the suspension of the solid samples in hexane directly onto holey-carbon-coated copper grids. HR HAADF-STEM and STEM-iDPC imaging was performed on a double-aberration-corrected, monochromated, FEI Titan3 Themis 60–300 microscope working at 300 kV. The last technique, iDPC imaging, provides in this microscope atomically resolved images in which the contrasts are related to the atomic number of the elements under the beam, instead of the roughly  $Z^2$ -dependent contrasts obtained in HAADF-STEM images. By using a four-segment detector, this technique allows imaging light elements, such as O, in the presence of heavier ones (Si,  $Z = 14$ ) under very low-electron-dose conditions, a key aspect in the atomic-scale structural analysis of zeolites, which are very sensitive to electron beams. In particular,  $2048 \times 2048$  HAADF iDPC image pairs were recorded simultaneously using a convergence angle of 18.6 mrad and a camera length of 91 mm. This configuration allowed us to optimize the collection of the signals on the HAADF and FEI DF4 detectors. To limit the damage by the electron beam, a fast image-recording protocol was used by combining a beam current of 30 pA, a 2.5  $\mu\text{s}$  dwell time and an automated fine-tuning alignment of A1 and C1 using the OptiSTEM software. To obtain images with good quality, the beam current and image acquisition time should be optimized according to the stability of the sample under the beam.

The microscope was also used to perform chemical mapping at medium magnifications (approximately 100k to 200k) by STEM-XEDS using the high-efficiency SuperX G2 detection system equipped in the microscope, which integrates four windowless detectors surrounding the sample and high-performance signal-processing hardware. STEM-XEDS was used to map the spatial distribution of Al, Si, Na and I elements. For this nanoanalytical experiment, the beam current was increased to 100 pA and the dwell time

to 128  $\mu$ s to obtain a good signal-to-noise ratio. Then, the elemental maps were background subtracted and smoothed by 3 pixel  $\times$  3 pixel averaging.

### **Catalyst preparation.**

**General preparation of basic zeolites.** X and Y zeolites, in  $\text{Na}^+$  form, are commercially available. These zeolites were treated with 0.1 M aqueous solutions of KOAc or CsOAc, typically at 70  $^{\circ}\text{C}$  for 24 h, to give the corresponding KY, KX and CsX zeolites. The extent of this first exchange is typically 65% and 25% for  $\text{K}^+$  and  $\text{Cs}^+$ , respectively. Two more exchanges were carried out in order to increase the total cation exchange to 75% and 36% for  $\text{K}^+$  and  $\text{Cs}^+$ , respectively.

**General preparation of acid zeolites.** H-Y and H-Beta zeolites are both commercially available. The NaY zeolite was treated with an aqueous solution of  $\text{LiNO}_3$  to give the corresponding LiY zeolite. The exchange took place at 60  $^{\circ}\text{C}$ . The exchange achieved was a 70% of  $\text{Li}^+$ .<sup>1</sup>

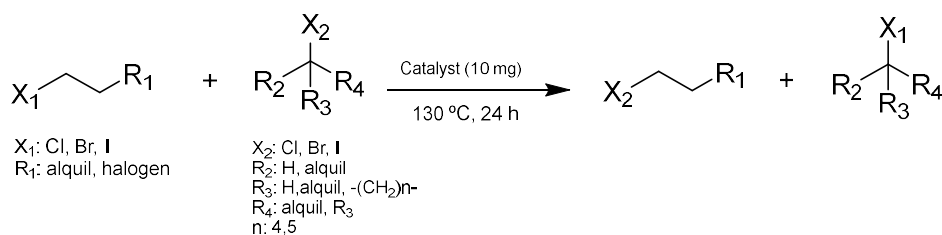
**Preparation of Na-Beta zeolite.** A 1M aqueous solution of  $\text{NaNO}_3$  was prepared. Then H-Beta zeolite was mixed with the solution in a ratio 1:10 for 4 h at 80  $^{\circ}\text{C}$  and, after that, filtered in vacuum. The procedure was repeated 3 times. Finally, the zeolite was dried under vacuum overnight.<sup>2</sup> ICP analysis showed 5.00 wt% Na in Na-Beta.

**Preparation of K-Beta zeolite.** The same procedure than for Na-Beta was followed, but this time using  $\text{CH}_3\text{COOK}$ . ICP analysis showed 3.01 wt% of K in K-Beta.

**Preparation of Na-SiO<sub>2</sub>-Al<sub>2</sub>O<sub>3</sub>.** A 1M aqueous solution of  $\text{NaNO}_3$  was prepared. SiO<sub>2</sub>-Al<sub>2</sub>O<sub>3</sub> was mixed with the solution in a ratio 1:10 for 4 h at 80  $^{\circ}\text{C}$  and, after that, filtered in vacuum. The procedure was repeated 3 times. Finally, the zeolite was dried under vacuum overnight.<sup>2</sup>

**Preparation of K-SiO<sub>2</sub>-Al<sub>2</sub>O<sub>3</sub>.** Same procedure than for Na-SiO<sub>2</sub>-Al<sub>2</sub>O<sub>3</sub> was followed, but this time using  $\text{CH}_3\text{COOK}$ .

### Typical reaction procedure in batch.



**Scheme S1.** Halogen exchange reaction conditions.

Products were obtained following the reaction Scheme S1. Reagents (1 mmol and 5-10 eq., respectively) were introduced in sealed vials with a magnetic stirrer and then the solid catalyst (10 mg, unless otherwise indicated). The mixture was allowed to react for 1 to 3 days at 130 °C and atmospheric pressure. GC samples were prepared introducing 25 µL of the reaction mixture in a vial with 1 mL of DCM and *N*-dodecane as an external standard.

### Calculation of the space-time yield (STY).

Flow reactor: 2 g of solid catalyst, 0.1 mL·min<sup>-1</sup> flow rate, 6 h reaction time, then 36 mL in total during 6 h.

Result: 30 mmol of limiting reactant with a 90.7% of conversion gives 27.21 mmol of product. Catalyst volume is 3.88 mL (2 g) and time is 6 h:

$$STY = \frac{27.21 \cdot 10^{-3} \text{ mol}}{3.88 \cdot 10^{-3} \text{ L} \cdot 6 \text{ h}} = 1.16 \frac{\text{mol}}{\text{L} \cdot \text{h}}$$

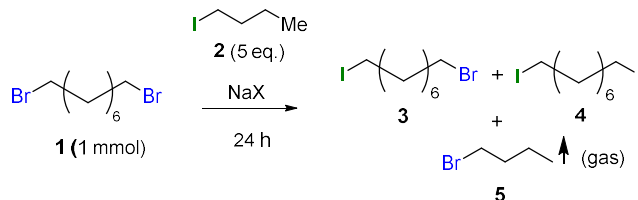
Batch reactor: 10 mg of solid catalyst, 24 h reaction time.

1 mmol of limiting reactant with a 99.0 % of conversion gives 0.99 mmol of product. Catalyst volume is 0.02 mL and time is 24 h.

$$STY = \frac{0.99 \cdot 10^{-3} \text{ mol}}{0.02 \cdot 10^{-3} \text{ L} \cdot 24 \text{ h}} = 0.21 \frac{\text{mol}}{\text{L} \cdot \text{h}}$$

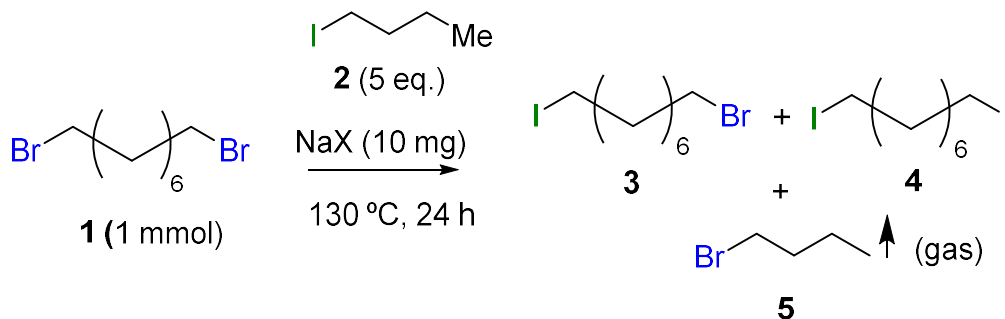
## Tables.

**Table S1.** Optimization of the reaction parameters for the halex reaction catalyzed by NaX. GC results.



Entry	Temperature (°C)	Catalyst (mg)	Conversion (%)
<b>1</b>	110	10	67.9
<b>2</b>	130		99.0
<b>3</b>	150		99.0
<b>6</b>	130	1	5.5
<b>7</b>		5	84.9
<b>8</b>		10	99.0
<b>9</b>		20	99.0

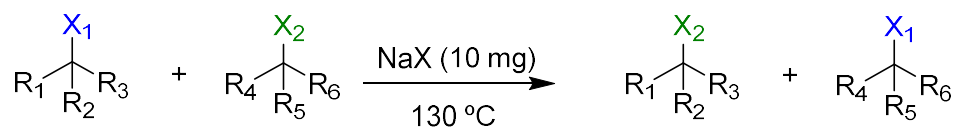
**Table S2.** Robustness test for the reaction substrate scope, using different functionalities for the reaction. GC results.



Entry	Reactant	Conversion (% , 24 h)	Selectivity to 3 (%)	Selectivity to 4 (%)
<b>1</b>		99	1	99
<b>2</b>		41	81	19
<b>3</b>		99	45	43

4		87	57	43
5		99	12	88
6		72	71	29
7		98	13	46
8		99	10	36
9		88	53	47

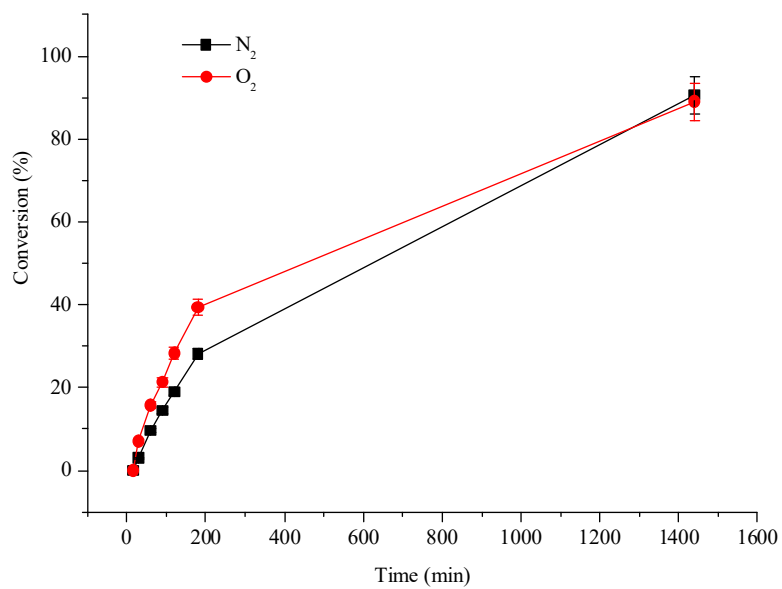
**Table S3.** Halex reaction between different aromatic halogenated compounds. GC results.



$\text{X}_1 = \text{X}_2 = \text{Cl, Br, I}$ ;  $\text{R}_{1-6} = \text{H, } n\text{-alkyl, } -(\text{CH}_2)_n\text{-, Bn with different functional groups.}$

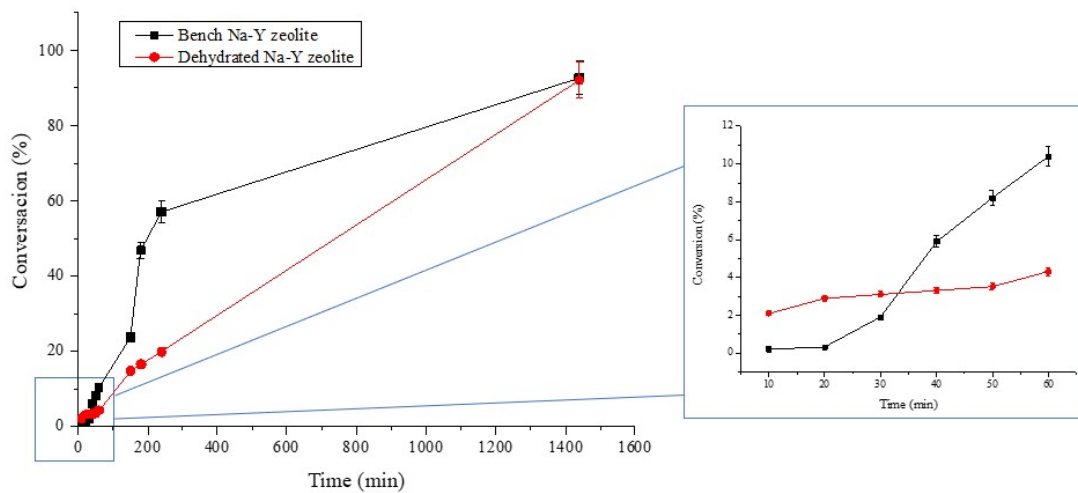
Entry	Reactant (1)	Reactant (2)	Conversion (%)
1			0.0
2			0.0
3			0.0

## Figures.

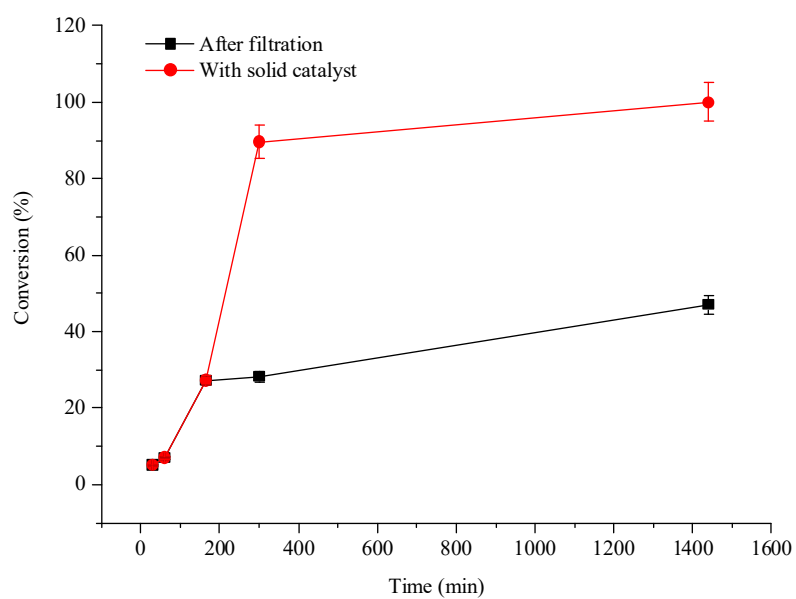


**Figure S1.** Kinetics for the halex reaction catalysed by NaY in the presence of an O<sub>2</sub> or N<sub>2</sub> atmosphere, for reaction conditions see Table 1 in the main text. Error bars account for a 5% uncertainty.

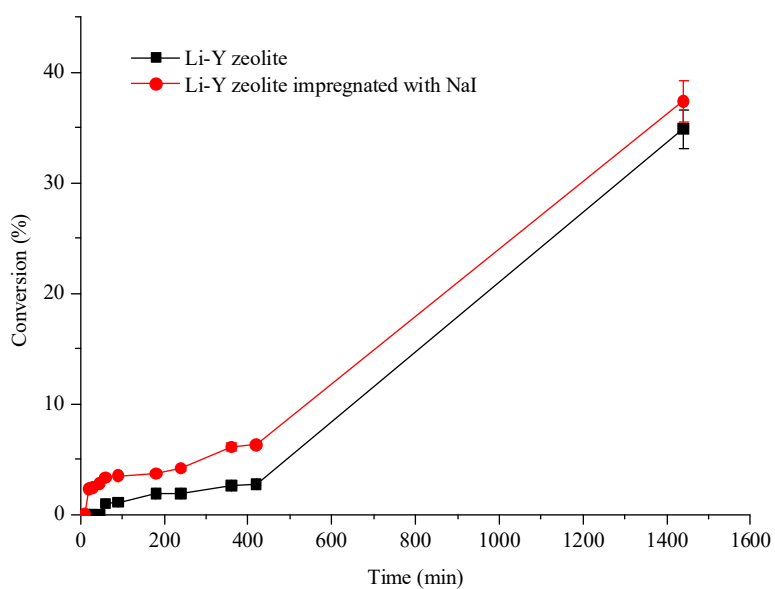
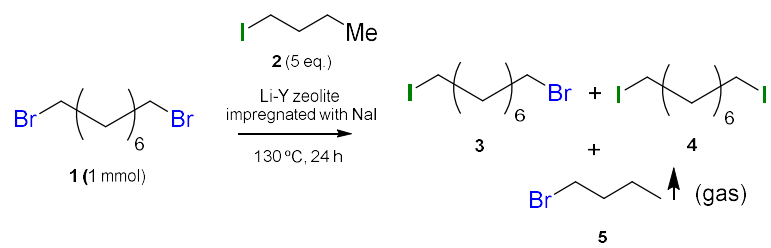




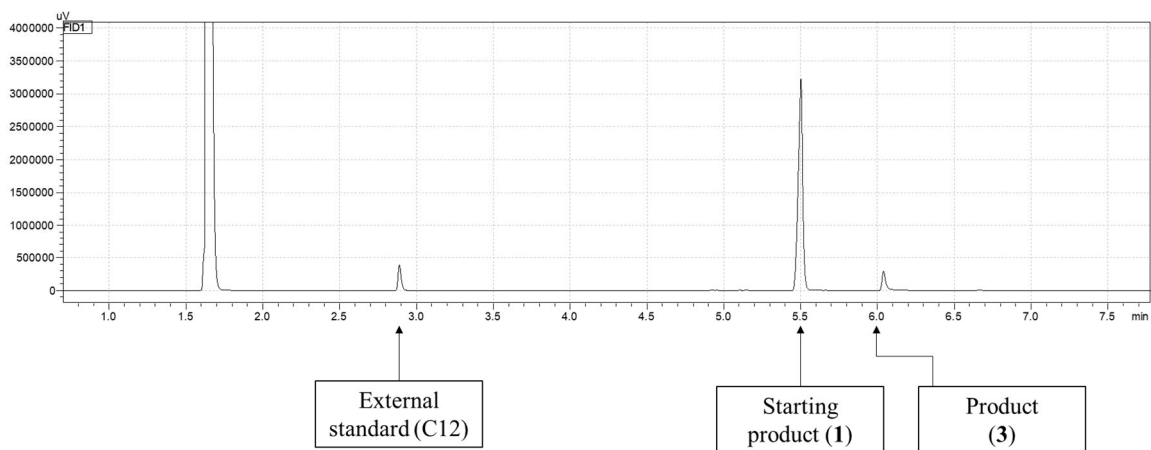
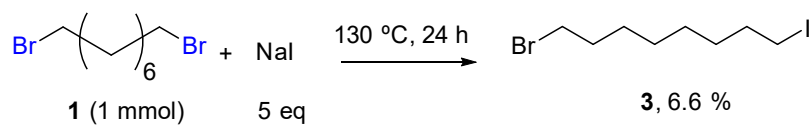
**Figure S2.** Kinetics for the halex reaction catalysed by bench and dehydrated Na-Y zeolite. Error bars account for a 5% uncertainty.



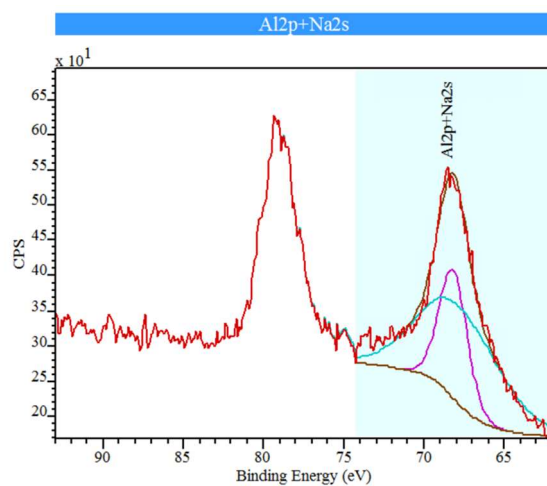
**Figure S3.** Leaching test for the halex reaction catalyzed by Na-Y zeolite, for reaction conditions see Table 1 in the main text. The hot filtration of the catalyst took place after 165 min. Error bars account for a 5% uncertainty.



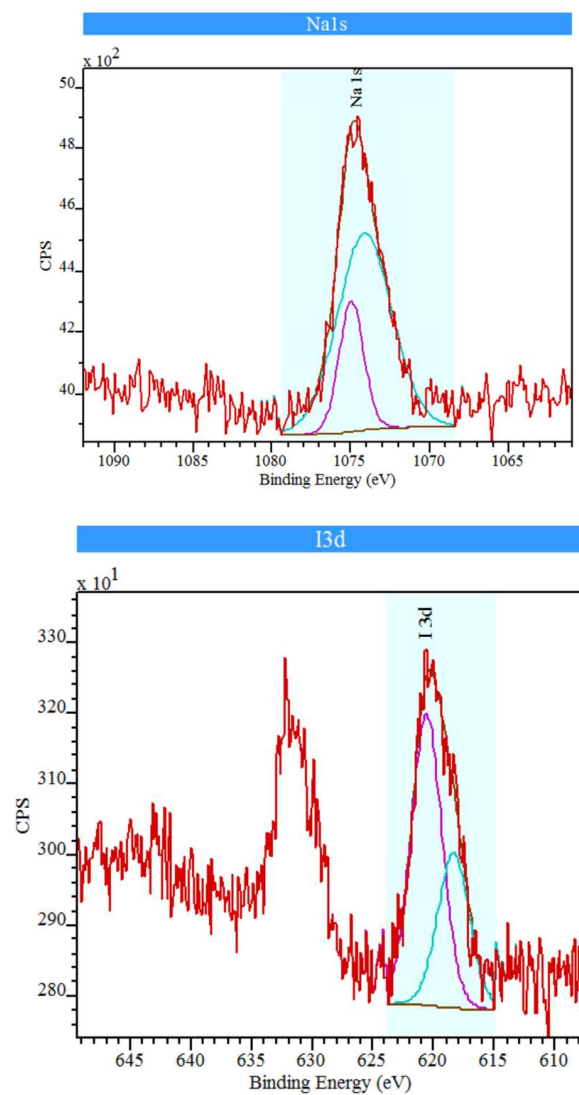
**Figure S4.** Kinetics for the halex reaction catalysed by Li-Y zeolite and Li-Y zeolite impregnated with NaI. Error bars account for a 5% uncertainty.



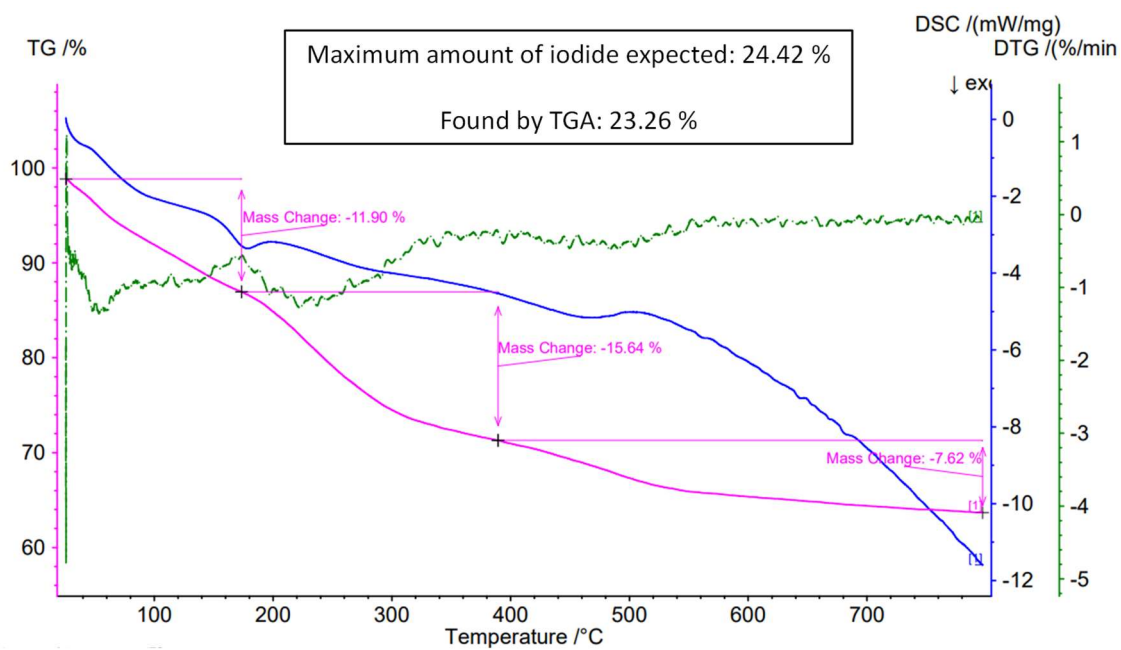
**Figure S5.** Control experiment with NaI, showing the corresponding GC spectrum.



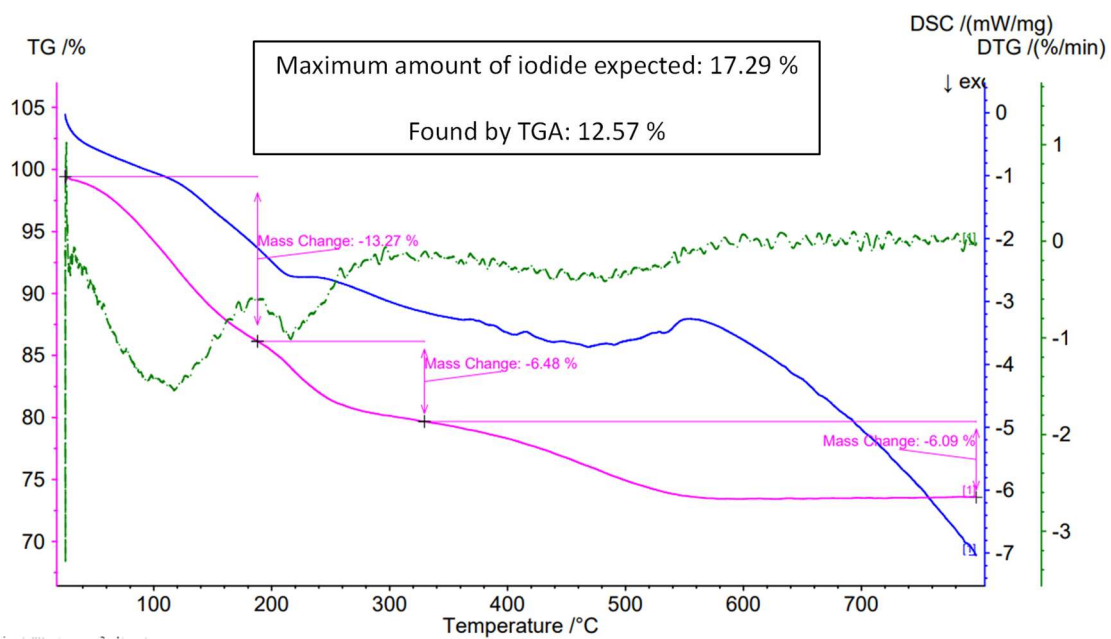
**Figure S6.** Deconvoluted Na 2s + Al 2p x-ray photoelectron spectroscopy (XPS) of NaX zeolite after reaction with iodobutane **2** at 130 °C. The blue area shows the deconvoluted part of the spectrum.



**Figure S7.** Deconvoluted Na  $1s$  (top) and I  $3d$  (bottom) X-ray photoelectron spectroscopy (XPS) of NaY zeolite after reaction with iodobutane **2** at 130 °C. The blue area shows the deconvoluted part of the spectra.

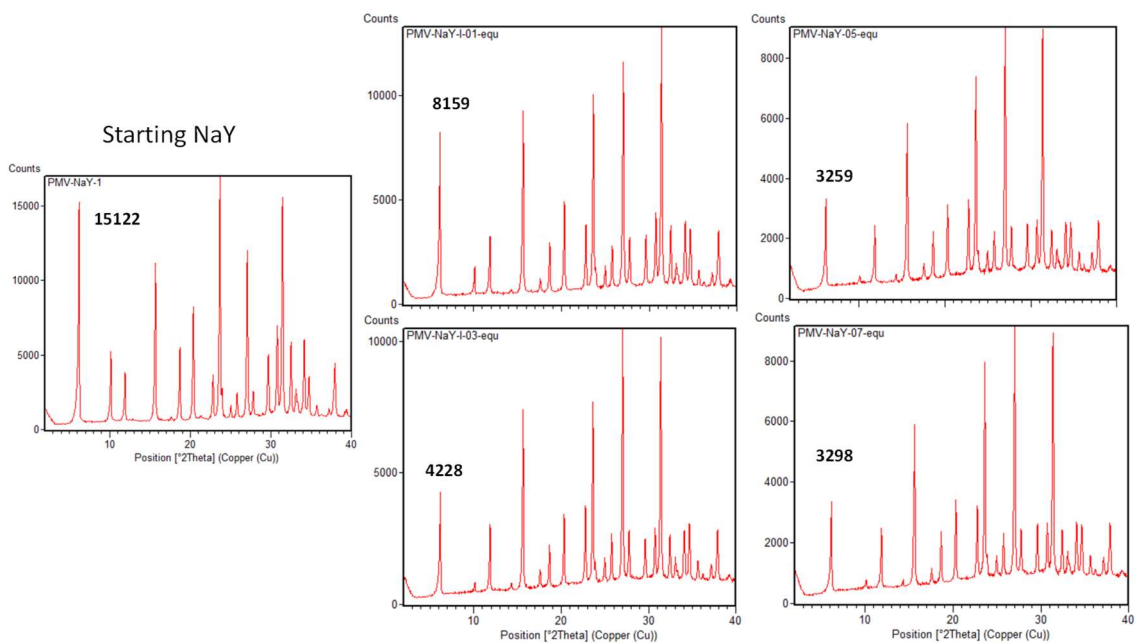


**Figure S8.** Thermogravimetric (TG) analysis of NaX after reaction with iodobutane **2** at 130 °C.

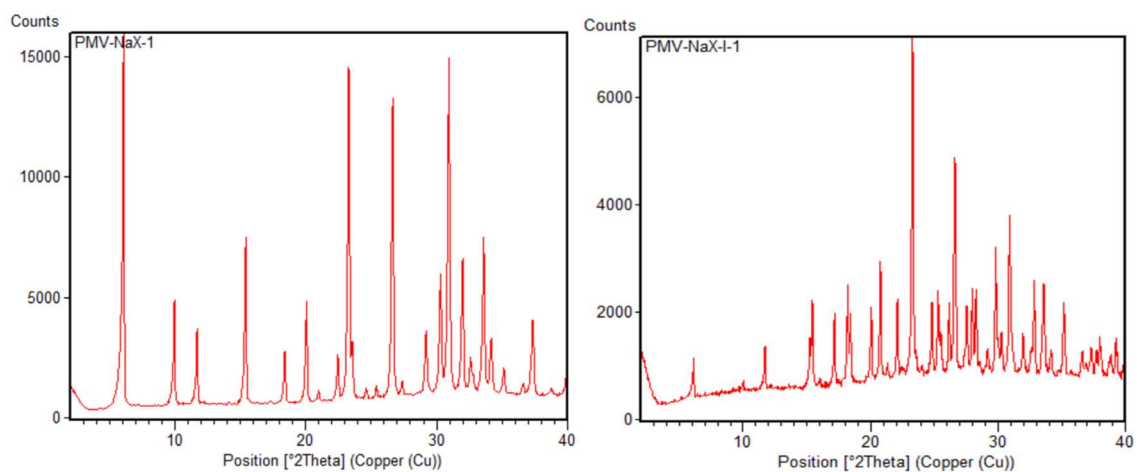


**Figure S9.** Thermogravimetric (TG) analysis of NaY after reaction with iodobutane **2** at 130 °C.

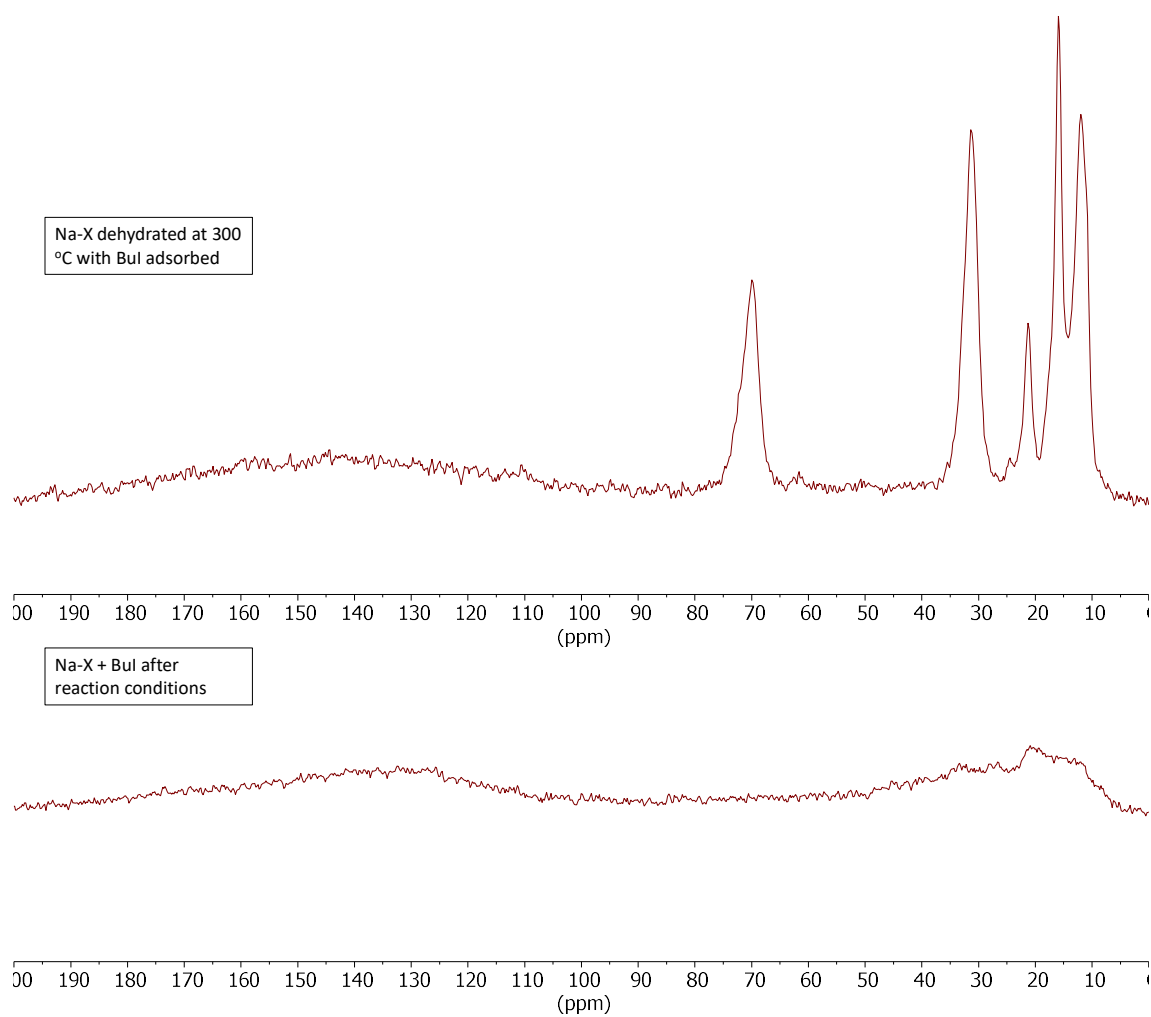




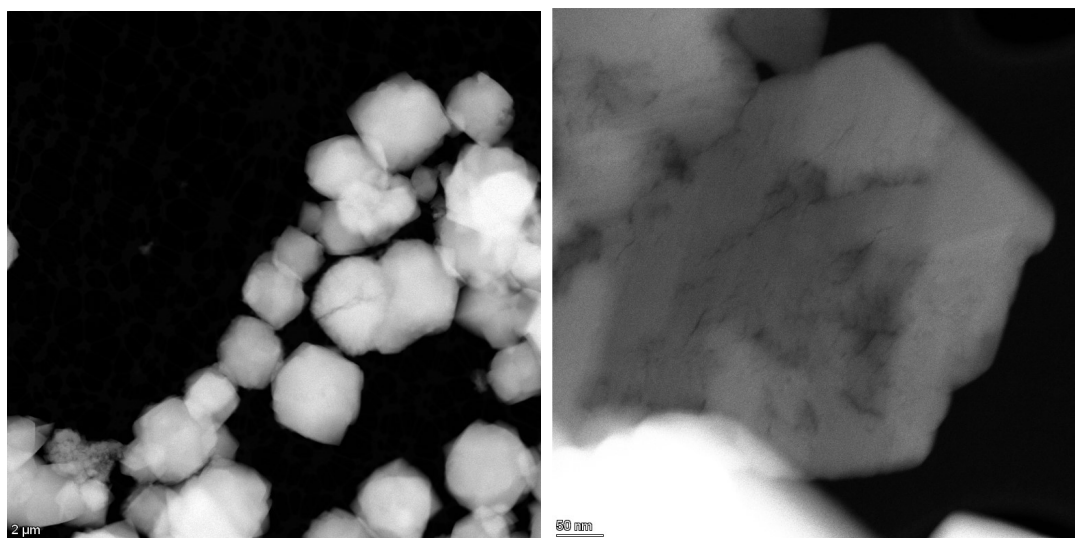
**Figure S10.** Powder X-ray diffraction (PXRD) measurements of NaY reacted with different amounts of organohalide **2** (from top to bottom: 0.1, 0.3, 0.5 and 0.7 mmol of **2**, respectively). The number above the signal at  $2\theta \sim 6^\circ$  is the intensity in counts.



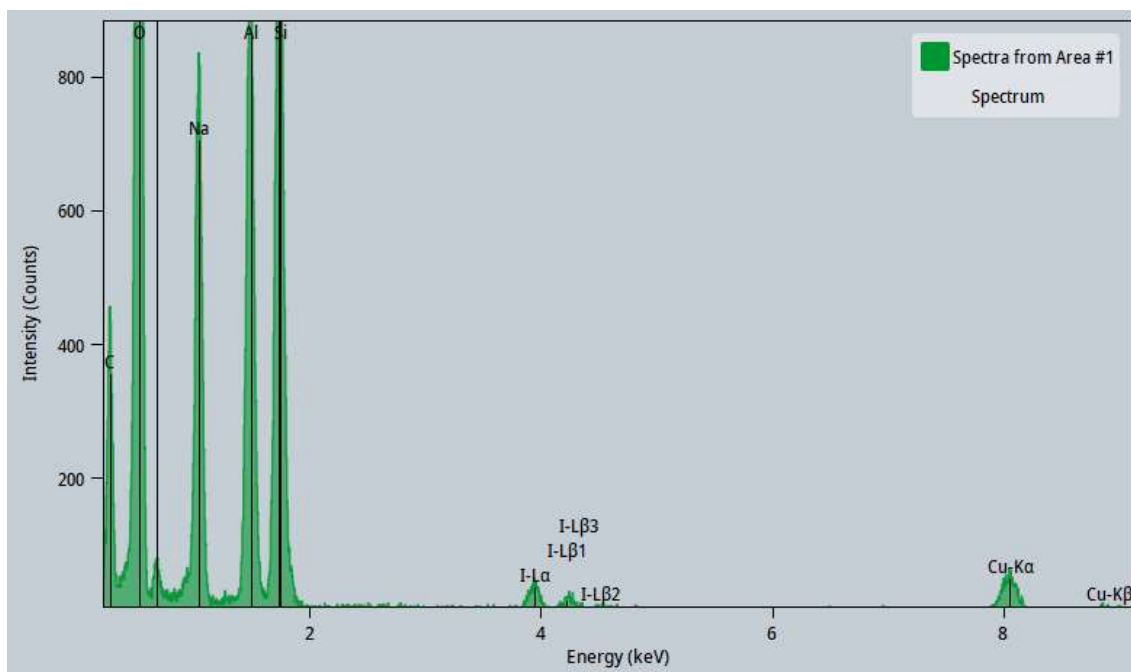
**Figure S11.** Powder X-ray diffraction (PXRD) measurements of fresh NaX (left) or reacted with organohalide **2** (excess, right).



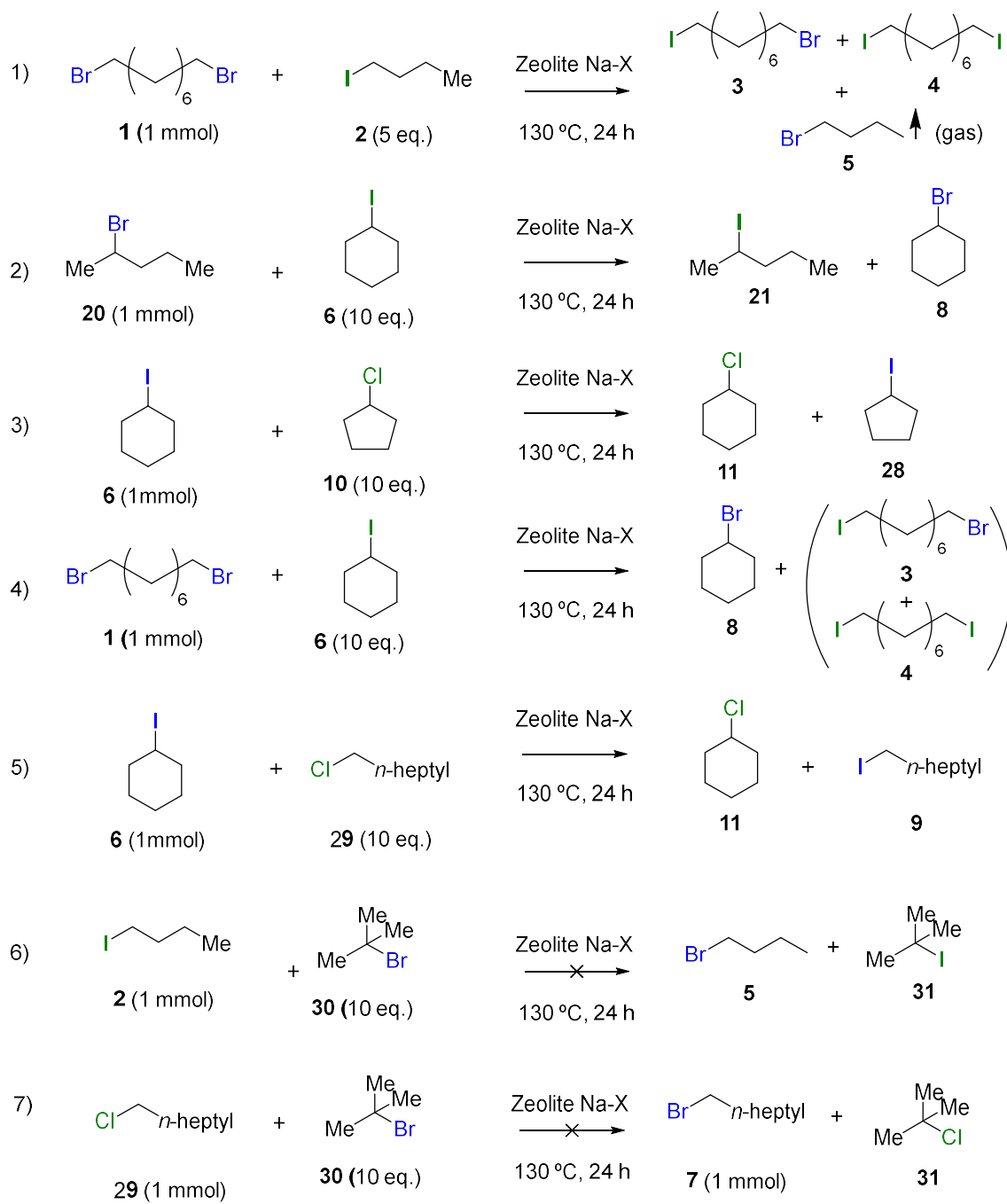
**Figure S12.**  $^{13}\text{C}$  NMR solid spectra of the Na-X zeolite with adsorbed BuI and after reacting at 130 °C.

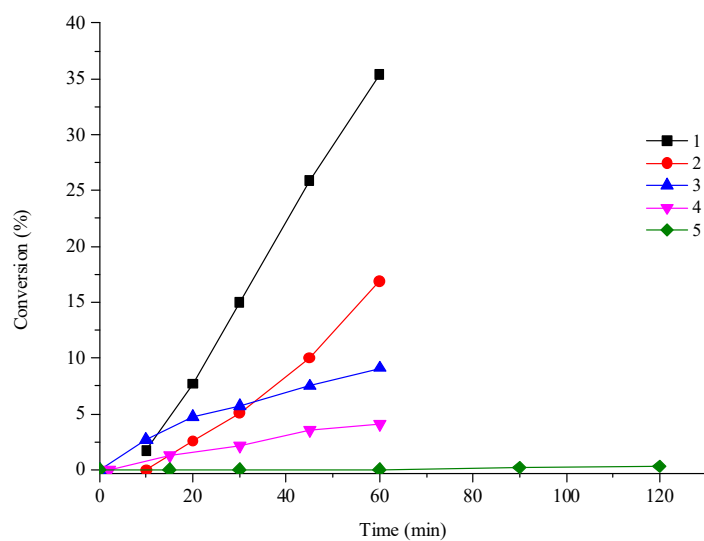


**Figure S13.** High-angle-annular-dark-field scanning transmission electron images (HAADF-STEM) of a NaX sample after reacting with BuI **2** at 130 °C.



**Figure S14.** Representative X-ray energy dispersive spectrum (EDS) of the zeolite particle shown in Figure 4 in the main text. The Cu signals correspond to the Cu grid employed for the measurement.

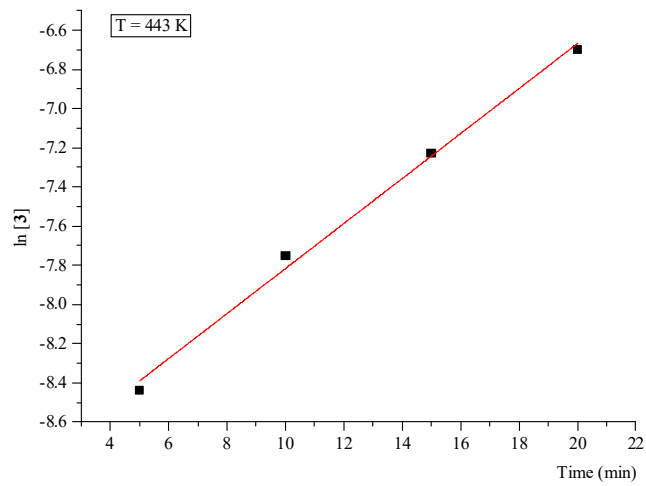
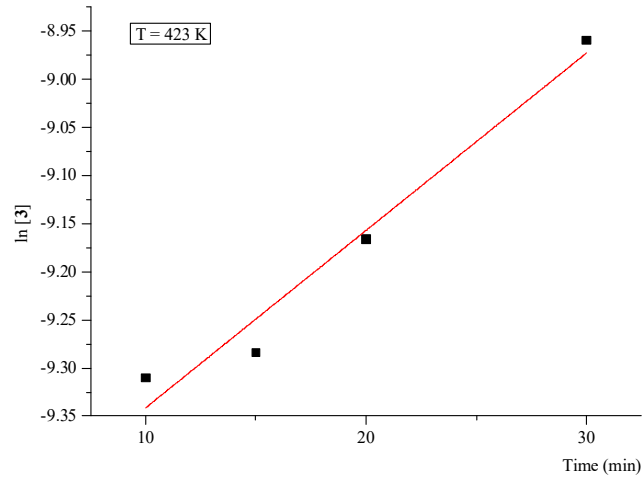
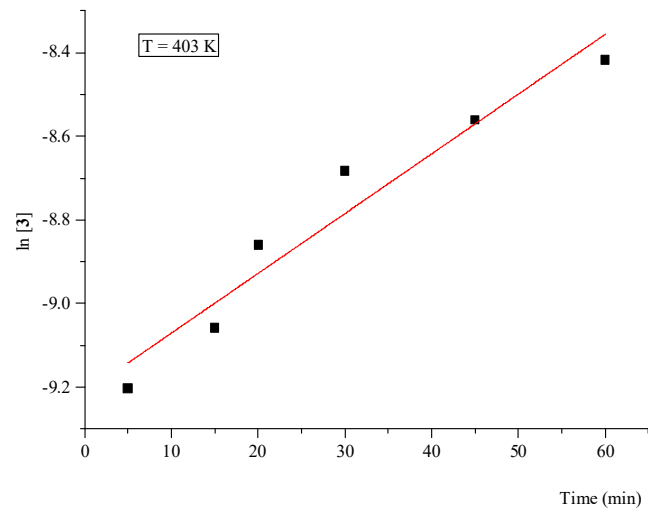




Reaction	Initial rate (% conv/ min)	Final conversion (%)
1	0.6861	93
2	0.3305	69
3	01417	16
4	0.0713	27
5	0.0061	4

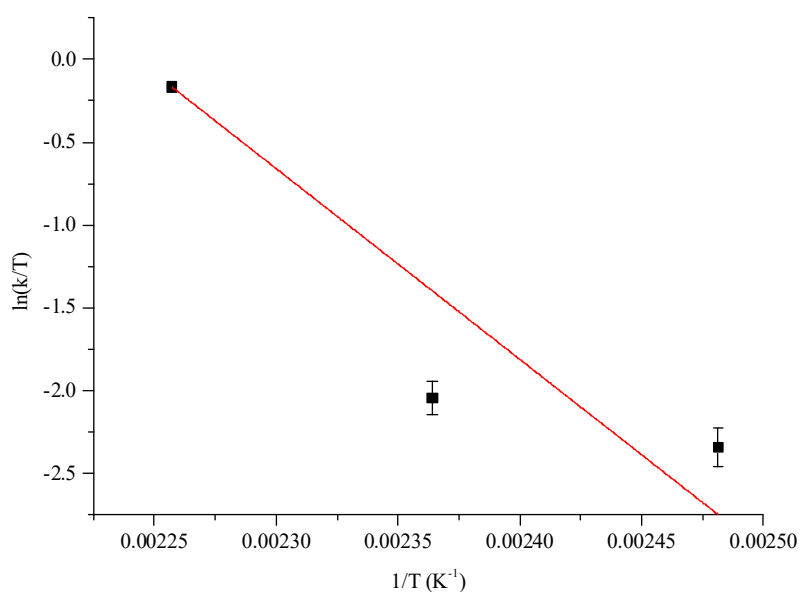
Initial rate:  $1^\circ \text{ Br} \leftrightarrow 1^\circ \text{ I} > 2^\circ \text{ Br} \leftrightarrow 2^\circ \text{ I} > 2^\circ \text{ Cl} > 1^\circ \text{ Br} \leftrightarrow 2^\circ \text{ I} > 2^\circ \text{ Br} \leftrightarrow 1^\circ \text{ Cl} > 1^\circ \text{ I} \leftrightarrow 3^\circ \text{ Br} \sim 1^\circ \text{ Cl} \leftrightarrow 3^\circ \text{ Br}$

**Figure S15.** Order of reactivity calculated for different primary, secondary and tertiary halogen exchanges, according to reactivity tests and compared kinetics.





$\ln(P) = k \cdot t + \ln(P)_0$			
T (K)	a = k	b = $\ln(P)_0$	R <sup>2</sup>
403	0.0143	-9.2134	0.9417
423	0.0184	-9.5257	0.9681
443	0.1148	-8.9652	0.9954



$\ln\left(\frac{k}{T}\right) = -\left(\frac{\Delta H^\ddagger}{R}\right)\frac{1}{T} + \left(\frac{\Delta S^\ddagger}{R}\right) + \ln\left(\frac{k_B}{h}\right)$		
$a = \left(\frac{\Delta H^\ddagger}{R}\right)$	$b = \left(\frac{\Delta S^\ddagger}{R}\right) + \ln\left(\frac{k_B}{h}\right)$	R <sup>2</sup>
-9600.9	21.214	0.8313

$$\Delta H^\ddagger = 19.08 \text{ kcal}\cdot\text{mol}^{-1}; \Delta S^\ddagger = -0.005 \text{ kcal}\cdot\text{mol}^{-1}\text{K}^{-1}$$

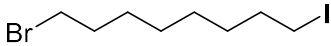
$$\Delta G^\ddagger = \Delta H^\ddagger - T\Delta S^\ddagger = 20.57 \text{ kcal}\cdot\text{mol}^{-1} \text{ (T= 298 K)}$$

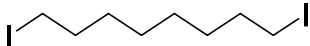
**Figure S16.** Eyring-Polanyi plot and energetic values in the transition state for the NaY zeolite-catalyzed reaction. Error bars account for a 5% uncertainty.

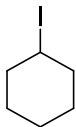
## References.

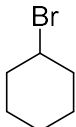
- 1 H. S. Kim, D. Bae, W. T. Lim and K. Seff, *J. Phys. Chem. C*, 2012, **116**, 9009–9018.
- 2 X. Xu, X. Zhao, L Sun, and X Liu, *J. Nat. Gas Chem.*, 2008, **17**, 391–396.

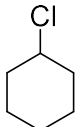
## Characterization of compounds.

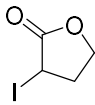
 *1-bromo-8-iodooctane (3)*. GC-MS (m/z, M<sup>+</sup>319), major peaks found: 320-318, 193-191, 111 (100%), 69, 55, 41, 27.

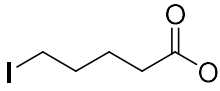
 *1,8-diiodooctane (4)*. GC-MS (m/z, M<sup>+</sup> 366), major peaks found: 366, 239, 183, 155, 111, 69 (100%), 55, 41.

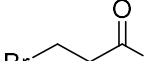
 *2-iodocyclohexane (6)*. GC-MS (m/z, M<sup>+</sup>210), major peaks found: 210, 83 (100%), 55, 41, 28.

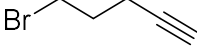
 *Bromocyclohexane (8)*. GC-MS (m/z, M<sup>+</sup>163), major peaks found: 164-162, 83 (100%), 67, 55, 41, 27.

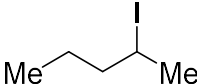
 *Chlorocyclohexane (11)*. GC-MS (m/z, M<sup>+</sup> 119), major peaks found: 120-118, 82 (100%), 67, 55, 41, 28.

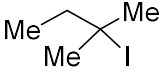
 *α-iodo-γ-butyrolactone (13)*. GC-MS (m/z, M<sup>+</sup>212), major peaks found: 213 (100%), 86, 69, 57, 41.

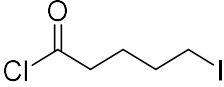
 *5-iodopentanoic acid (15)*. GC-MS (m/z, M<sup>+</sup>228), major peaks found: 211, 183, 101(100%), 83, 55, 43.

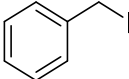
 **3-bromopropanoic acid (17)**. GC-MS (m/z, M<sup>+</sup> 153), major peaks found: 154-152 (100%), 137-135, 109-107, 73, 55, 45, 28.

 **5-bromo-1-pentyne (19)**. GC-MS (m/z, M<sup>+</sup> 147), major peaks found: 148-146, 67 (100%), 39.

 **2-iodopentane (21)**. GC-MS (m/z, M<sup>+</sup> 198), major peaks found: 198, 127, 71 (100%), 55, 43, 29.

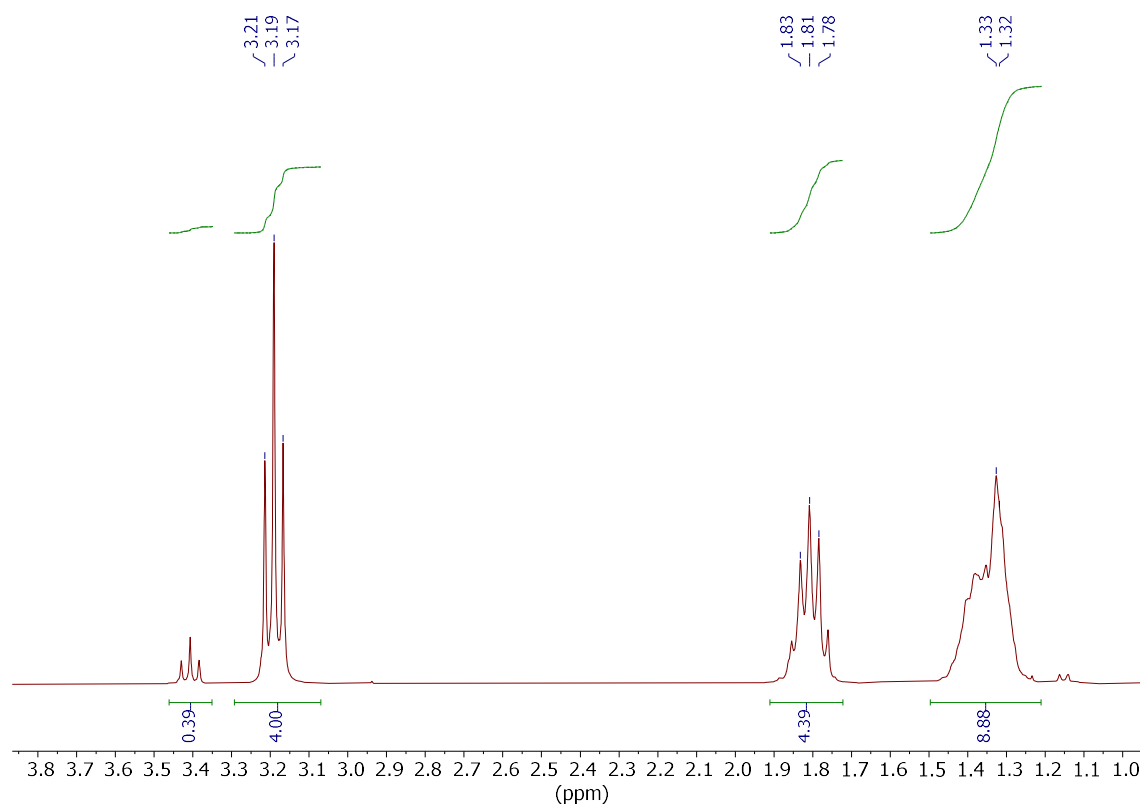
 **2-iodo-2-methylbutane (23)**. GC-MS (m/z, M<sup>+</sup> 198), major peaks found: 198, 127, 71 (100%), 55, 43, 28.

 **5-iodopentanoyl chloride (25)**. GC-MS (m/z, M<sup>+</sup> 247), major peaks found: 248-246 (100%), 127, 121-119, 65-63, 56.

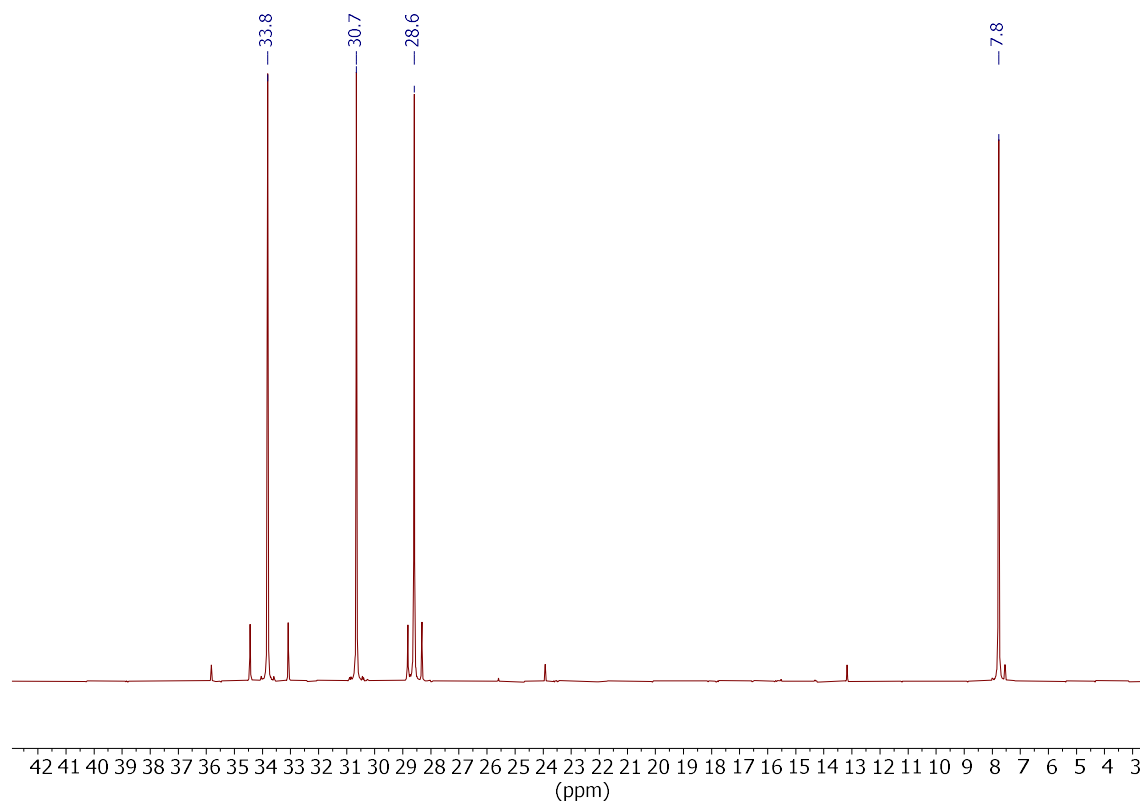
 **(Iodomethyl)benzene (27)**. GC-MS (m/z, M<sup>+</sup> 218), major peaks found: 218, 127, 91 (100%), 65.

NMR copy: 1,8-diiodooctane (**4**).

$^1\text{H}$  NMR 300 MHz



$^{13}\text{C}$  NMR 75 MHz



# DEPT

